Letter

Simultaneously improving Rashba-type and Zeeman effects in two-dimensional multiferroics

Xu Li,[1,2] Hao Tian,[1,2,3] Hong Jian Zhao,[4,5] Changsong Xu,[4,6] Meng Ye,[7] Lan Chen,[1,2,*] Hongjun Xiang,[6] Jun-Ming Liu,[1] L. Bellaiche,[4] Di Wu,[1,2,†] and Yurong Yang[1,2,‡]

[1]*National Laboratory of Solid State Microstructures and Collaborative Innovation Center of Advanced Microstructures, Nanjing University, Nanjing 210093, China*

[2]*Jiangsu Key Laboratory of Artificial Functional Materials, Department of Materials Science and Engineering, Nanjing University, Nanjing 210093, China*

[3]*School of Physics and Electronic Engineering, Zhengzhou Normal University, Zhengzhou 450044, China*

[4]*Physics Department and Institute for Nanoscience and Engineering, University of Arkansas, Fayetteville, Arkansas 72701, USA*

[5]*International Center of Computational Method and Software, College of Physics, Jilin University, Changchun 130012, China*

[6]*Key Laboratory of Computational Physical Sciences (Ministry of Education), State Key Laboratory of Surface Physics, and Department of Physics, Fudan University, Shanghai 200433, China*

[7]*State Key Laboratory of Low Dimensional Quantum Physics and Department of Physics, Tsinghua University, Beijing 100084, China*

(Received 19 November 2021; revised 18 April 2022; accepted 19 October 2022; published 10 November 2022)

First-principles calculations are performed to investigate Rashba-type and Zeeman effects in two-dimensional three-atom-layer structures XTe/MnTe/XTe (XMX, X = Sn, Ge). It is found that the Rashba-type and Zeeman effects that typically compete against each other rather cooperatively work together and are improved in XMX, as compared to XTe/XTe/XTe (XXX). This cooperation and improvement are highly required in Majorana qubits for topological quantum computing, Josephson junction of topological superconductivity, and other phenomena. The Rashba-type effect is improved because replacing XTe by MnTe leads to a reduction of the thickness of XMX and increases the interaction between the surface state of the lowest conduction bands and its neighboring states. The improved Zeeman effect in the XMX structure arises from *s-d* and *p-d* exchange interactions between Te and Mn ions. The present strategy of simultaneously largely improving Rashba-type and Zeeman effects therefore provides a route to realize stable Majorana fermions, topological superconductivity, and other phenomena that require both large Rashba-type and Zeeman effects.

DOI: 10.1103/PhysRevB.106.L201105

Typically, the degeneracy of spins is protected by the combination of spatial inversion and time-reversal symmetry. However, the Zeeman effect is a phenomenon in which the spin degeneracy is split by the time-reversal symmetry broken under external magnetic field. Furthermore, the Rashba-type effect is another phenomenon for which the spin degeneracy is lifted, thanks to the spin-orbit coupling (SOC) and via the breaking of the spatial inversion symmetry. Zeeman effect and Rashba-type SOC are the essential factors to form the Majorana qubit in the main platforms of quantum information processing [1–8], topological superconductivity in Josephson junction [9–11], optical cavities and spin-split photo mode [12], and spintronics [13,14]. However, Zeeman and Rashba-type effects are considered to be competitive because the former tends to align the spins by magnetic field while the action of the latter prevents the spins from reaching full alignment. This is somehow unfortunate because their intrinsic competition [5,15,16] can result in few materials possessing Majorana fermions, topological superconductivity, optical cavities, and so on. While the SOC is known to be tunable by gate and film thickness [17], here we report a way to simultaneously improve Zeeman and Rashba-type effects and therefore reduce their competition.

We propose a strategy to accomplish this dual improvement in two-dimensional (2D) sandwich multiferroics in this Letter. More precisely, we conducted first-principles calculations on the three-atom-layer structures XTe/MnTe/XTe (XMX, X = Sn, Ge) made by polar XTe and antiferromagnetic MnTe layers. Comparing to the pure three XTe structure (i.e., the XTe/XTe/XTe structure), both Rashba-type and Zeeman effects are improved in XMX. The improvement of the Rashba-type effect is due to the fact that the thin XMX structure gives a strong interaction between surface states and interior states, leading to the shift and change of the electronic structure. The enhanced Zeeman effect in XMX originates from the *s-d* and *p-d* exchange interaction between Te and Mn.

Here, first-principles calculations based on density functional theory are performed, using the projector augmented wave method [18] as implemented in the Vienna *Ab initio* Simulation Package (VASP) [19–21]. The exchange-correlation potential is described by the Perdew-Burke-Ernzerhof functional of the generalized gradient approximation [22] with a Hubbard U correction for better treatment on Mn [23,24]. We use U values of 2.6 and 3.0 eV on Mn for GeTe/MnTe/GeTe (GMG) and SnTe/MnTe/SnTe (SMS),

*chenlan@nju.edu.cn
†diwu@nju.edu.cn
‡yangyr@nju.edu.cn

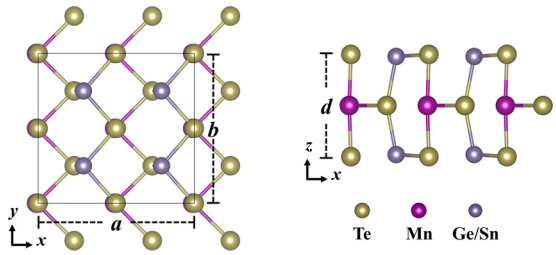

FIG. 1. Structure of XMX. The left and right panels show the top and side view, respectively. Note that there are four Mn ions in the supercell, which is represented by a rectangle.

respectively. The reason for choosing such U on Mn ions and other details of calculations can be found in the Supplemental Material [25] (see, also, Refs. [26–36] therein).

It was found in the literature that 2D SnTe with a few atomic layers adopts ferroelectricity [37], while the 2D MnTe and MnSe layers present ferromagnetic properties [38,39]. SnTe and GeTe not only have similar rhombohedral $R3m$ structures at ambient condition, but also have similar orthorhombic $Pnma$ at high pressure [40–46]. From our calculations (see Fig. S1 in the Supplemental Material), the orthorhombic phase has lower energy than the hexagonal phase for few-layer structures for SnTe, GeTe, and MnTe, implying that SnTe, GeTe, and MnTe should adopt the orthorhombic phase when they have few layers. One may thus wonder if 2D structures having both SnTe (or GeTe) and MnTe layers can give rise to both ferroelectric and ferromagnetic (antiferromagnetic) properties. Here, we consider a three-layer structure of XMX made by one XTe layer on top, one MnTe atomic layer in the middle, and another XTe layer on the bottom. We predict that it adopts an orthorhombic *polar* point group C_{2v} (see Fig. 1), which combined with magnetism associated with Mn cations, enable these three-layer XMX structures to be novel 2D multiferroic (see Fig. S2 and Table S1 in the Supplemental Material).

The electric dipoles per area of GMG and SMS are 4.2×10^{-10} C/m and 4.4×10^{-10} C/m along a (or x) direction, respectively (see Fig. 1). Note that if we divide these numbers by the thickness of the 2D structure [47], indicated in Table I, the corresponding polarization would be 49.2 and 50.5 μC/cm^2 for GMG and SMS, respectively, which is even larger than that of prototypical ferroelectrics $BaTiO_3$

TABLE I. Parameters characterizing Rashba-type and Zeeman splittings. E_R (in meV) and α_R (in eV Å) are Rashba energy and Rashba parameter for lowest conduction bands, respectively. $g^*_{\beta\alpha}$ (where $\beta = v, c$ represents valence band and conduction band, and $\alpha = a, c$ is the direction along which the magnetic field is applied) is the Zeeman effective g factor. d (in Å) is the thickness of the corresponding 2D structures.

	E_R	α_R	d	g^*_{va}	g^*_{vc}	g^*_{ca}	g^*_{cc}
GMG	1.9	0.25	5.75	−4.31	5.22	−6.39	−7.67
GGG	0.5	0.14	5.92	−1.85	−1.91	−1.93	−1.97
SMS	48.9	2.69	5.81	−3.38	3.81	−0.53	−0.09
SSS	2.2	0.34	6.28	−1.79	−1.84	−1.74	−1.59

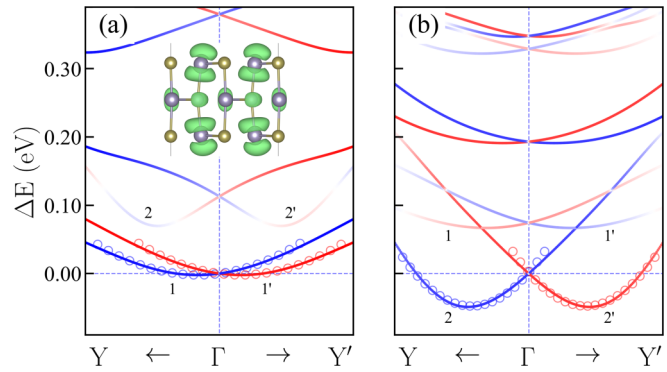

FIG. 2. The band structure of (a) SSS and (b) SMS. The inset of panel (a) displays the charge distribution of the CBM for SSS. Empty circles represent the fitted data by Eq. (2). The energy of cross-point of CBM is set to zero.

(26μC/cm^2) [48]. The electric dipoles per area of GMG and SMS are comparable to that of two atomic layers GeTe, SnTe, and three layers GeTe (GGG), SnTe (SSS). The magnetic ground states for GMG and SMS are found to be antiferromagnetic (see details in the Supplemental Material) with the local magnetic moment at Mn about 4.4 μ_B. Noncollinear magnetism calculations predict that both GMG and SMS have an easy magnetic axis along b, therefore perpendicular to their polarization. These multiferroic materials also exhibit a novel magnetoelectric phenomenon where the antiferromagnetic vector could be switched by 180° following the rotation of polarization under electric field (see the Supplemental Material).

Let us now turn our attention to the electronic structure of the XMX structure. For the C_{2v} point group, the Rashba-type splitting occurs along reciprocal k directions being perpendicular to its polarized in-plane x axis, with the Rashba-type SOC Hamiltonian written as [49–51]

$$H = H_0 + \alpha k_y \sigma_z + \beta k_z \sigma_y = H_0 + \alpha k_y \sigma_z, \tag{1}$$

where σ_i ($i = x, y, z$) are the Pauli spin matrices. Note that k_z should be neglected in our 2D structure, and the Rashba-type splitting thus occurs along k_y. The eigenvalues of Eq. (1) can be easily written as

$$E_\pm = E_0 \pm \alpha k_y. \tag{2}$$

From Eq. (1), Rashba-type splitting only occurs for k_y with spin vector along the z direction (i.e., σ_z). Figure 2 shows the band structure along the path Y-Γ-Y' for SSS and SMS calculated with SOC (see Fig. S6 for more details of the band structures). Rashba-type splitting in lowest conduction bands can be clearly found near the Γ point. Very interestingly, Rashba-type splitting in SMS is greatly enhanced, as compared with that in SSS. As a matter of fact and as shown in Table I, E_R for SMS is 48.9 meV, which is about 20 times larger than the 2.2 meV value for SSS. Consequently, the Rashba parameter $\alpha_R = 2E_R/k_0$ for SMS is equal to 2.69 eV Å while that of SSS is 0.34 eV Å. Note that the spin splitting in lowest conduction bands can be well fitted by $E = \beta' k_y^2 \pm \alpha k_y$, where the β' and α are the effective mass and linear spin-splitting terms (Rashba parameter), respectively. This proves that Eq. (2) is valid for fitting the first-principles

data. Note also that the Rashba parameter of 2.69 eV Å for SMS is one of the maximal Rashba parameters ever reported in 2D materials [52], and is even comparable to large values in bulk Rashba semiconductors such as BiTeI, etc. [53–56], to the best of our knowledge. As shown in Table I, Rashba energy E_R and Rashba parameters α_R for the GMG structure are also largely enhanced by almost four times and two times, respectively, with respect to GGG.

To understand the very large enhancement of Rashba-type effect in SMS and GMG, we carefully studied their electronic and atomic structures. As shown in the inset of Fig. 2(a), the CBM of the SSS structure near Γ is a surface state mainly displaying the p_z orbitals from Sn ions. Note that the conduction band minimum (CBM) for the SMS structure is also a surface state but possessing p_y orbitals characteristic from Sn ions (GMG possesses a similar characteristic as shown in Fig. S6). The energy levels of surface states are sensitive to their interaction with interior states and the thickness of 2D materials. As a Mn ion has less electrons (especially p_z electrons) than Sn, XMX with a MnTe layer in the middle (see Fig. 1) is thinner than SSS or GGG. This is confirmed by the structural calculations indicating that the thickness d of SMS is reduced by 0.47 Å and that for GMG is reduced by 0.17 Å (see Table I). The decrease of thickness of the 2D structure leads to the increase of interaction between surface states and interior states, resulting in the energy level of p_z surface states of 1 and 1′ [the two lowest conduction bands in Fig. 2(a)] shifting to higher energy, while the energy level of p_y surface states of 2 and 2′ shifts to lower energy [see Figs. 2(a) and 2(b)]. These shifts lead to 2 and 2′ bands becoming the lowest energy bands (see Fig. S8 for more information), and bands 2 and 2′ have larger Rashba-type effect than bands 1 and 1′, which is one factor explaining why the SMS structure possesses largely enhanced Rashba-type effect, as compared to the SSS structure. Regarding GMG, it possesses the same lowest conduction bands as GGG (see Fig. S7), and the new lowest conduction bands 2 and 2′ in SMS also explain why there are larger Rashba-type effects in SMS than in GMG.

Furthermore, there are other reasons for the Rashba-type splitting of XMX to be larger than that in XXX (see Fig. 2 and Fig. S7): there are more bands near the Fermi level and the bands are closer to each other in XMX. As a matter of fact, from second-order perturbations, the Rahsba energy can be written as [56,57]

$$\Delta\varepsilon_m^2(\mathbf{k}) = \frac{\hbar}{m_0}\sum_{n\neq m}\frac{\langle u_m \mid H \mid u_n\rangle\langle u_n \mid \mathbf{q}\cdot\mathbf{p} \mid u_m\rangle + \text{c.c.}}{\varepsilon_m - \varepsilon_n}, \quad (3)$$

where u_i and ε_i are the eigenstate and eigenenergy corresponding to the state i at $\mathbf{k_0}$, respectively, $\mathbf{q} = \mathbf{k} - \mathbf{k_0}$, $\mathbf{p}$ denotes the momentum operator, H is the corresponding Hamiltonian for Rashba-type splitting, and c.c. stands for the complex conjugation. From Eq. (3), the spin splitting is clearly dependent on the energy difference between neighboring states m and n. For the SMS in Fig. 2(b), the energy difference between the lowest conduction band state and its first nearest neighboring state at Γ is much smaller than that of SSS in Fig. 2(a). Similarly, the energy difference between the lowest conduction bands and its second nearest neighboring state at Γ for SMS is also smaller than that in SSS (note that GMG shows similar characteristics as shown in Fig. S7). These energy differences further lead to the enhancement of the Rashba-type effect in SMS according to Eq. (4). We are therefore proposing a strategy to enhance the Rashba-type effect in 2D structures by increasing the interaction between neighboring states [58].

Figure 3 shows the spin texture of states of the lowest conduction band at Γ and Y points in GMG. Strikingly, In Fig. 3(a), spin vectors are parallel/antiparallel to each other and independent on the k. This is the so-called persistent spin texture [59], consistent with the symmetry of the considered 2D structures and Eqs. (1) and (2), by which the spin vector of the states has only a z component and zero x and y spin components. On the other hand, the situation changes when an out-of-plane electric field is applied. As shown in Figs. 3(b) and 3(c), an in-plane Dresselhaus-like spin texture happens near the Γ point and an in-plane Rashba-like spin texture occurs at the Y point under external electric field 0.1 V/Å (note that other magnitudes of electric field give similar spin textures). This persistent spin texture being manipulated to in-plane Dresselhaus and Rashba spin textures, is very useful and important for the spin anisotropy and spin relaxation in spintronics [13,14,60,61] and optical cavities [12].

We then study the Zeeman effect, which is usually competitive with Rashba-type effect with large SOC. The spin splitting under magnetic field applied along in-plane directions a, b are first considered. The band splitting occurs only at the Γ point. In other words, the magnetic field opens an additional gap at Γ for both the lowest conduction band and the highest valence band (see Fig. S9). Under magnetic field along b, the effective g factor (g^*) of Zeeman effects ($\Delta E_Z = g^*\mu_B B$) for XMX is similar to that of SSS or GGG. On the other hand, under magnetic field applied along the a direction, it is greatly enhanced. As shown in Table I, g^* of XMX at both the lowest conduction band and the highest valence band are enhanced by two to three times with respect to SSS and GGG. More interestingly, under magnetic field lying along the c direction, the band splitting occurs not only at the Γ point, but also inside the Brillouin zone near Γ, where (i) the spin-up channel valence and conduction bands shift closer to each other, resulting in a small spin-up channel band gap, and (ii) spin-down channel valence and conduction bands shift far away from each other, yielding a large spin-down channel band gap. As shown in Fig. 4, the band along Γ-Y and Γ-Y' is asymmetric under magnetic field along the c direction. Figure 4(b) shows the Zeeman-splitting energy ΔE_Z (the energy difference between spin-up and spin-down channels induced by magnetic field) as a function of magnetic field. g^* (which is the slope of the approximately linear ΔE_Z-versus-B_z curve) of valence band maximum (VBM) and CBM for the GMG structure is −7.67 and 5.22 (see Table I), which are remarkably increased by 289% and 365%, respectively, as compared to the corresponding values in GGG. Note also that these effective g^* factors are comparable to the large g^* values reported in InAs and GaSb [62].

In order to understand the largely enhanced Zeeman effects in GMG, the projected band structure from Te and Mn ions is displayed in Figs. 4(c) and 4(d). One can see that conduction bands show s-d exchange interaction between Te s and Mn d orbitals while the valence bands involve p-d exchange interaction between Te p and Mn d orbitals. These

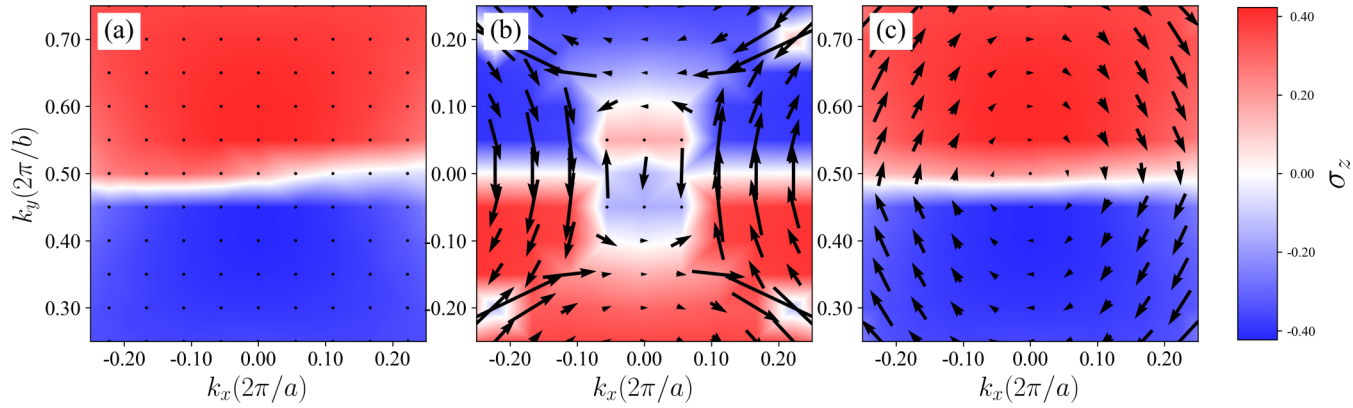

FIG. 3. Spin texture of the outer branch of the lowest conduction bands for GMG around Γ [panels (a) and (b)] and Y (0.0, 0.5, 0.0) [panel (c)] points. Panel (a) shows the spin texture at zero external electric field. Panels (b) and (c) display the spin texture at an electric field of 0.1 V/Å. The black arrows represent the in-plane spin component, while the blue and red colors represent the out-of-plane spin component.

s-d and *p-d* exchange interactions lead to the enhancements of Zeeman effect because of the large orbital angular momentum, which also occurred in Mn-doped CdSe and ZnSe/CdSe nanostructures [63,64]. More interestingly, the sign of ΔE_Z and g^* for the VBM in GMG is positive, which is thus inverted from the negative sign for the VBM in GGG [see Fig. 4(b)]. We are going to demonstrate it from the exchange interaction between Te and Mn. One can see that Te and Mn states in conduction states [see Figs. 4(c) and 4(d)] are both spin-up channels, indicating the potential (ferromagnetic) *s-d* exchange interaction, similar to the bulk II-VI diluted magnetic semiconductor [65,66]. While in valence states, states in Te and Mn belong to different spin channels, their *p-d* exchange interaction is kinetic type (antiferromagnetic) [64]. The kinetic-type (antiferromagnetic) *p-d* exchange interactions lead to the inverted sign of g^*_{vc} in GMG and in GGG. We also investigated the Zeeman effect in SMS and SSS (see Fig. S11). The largely enhanced Zeeman effect is also found for the VBM in SMS, while it is very small and reduced in the CBM in SMS. Electronic structure analysis shows that there are Mn *d* contributions in the VBM but none in the CBM (see Fig. S10), and therefore the large enhancement of the Zeeman effect in the VBM results from *s-d* exchange interaction while no enhancement happens for the CBM due to the lack of *p-d* exchange interaction. Note also that the Rashba-type effect of CBM in SMS is largely increased by about ten times, with respect to that in SSS (see Table I); this may be another reason for the reduction of Zeeman effect of CBM in SMS, since there is typically a competition between the Zeeman effect and the Rashba-type effect with large SOC.

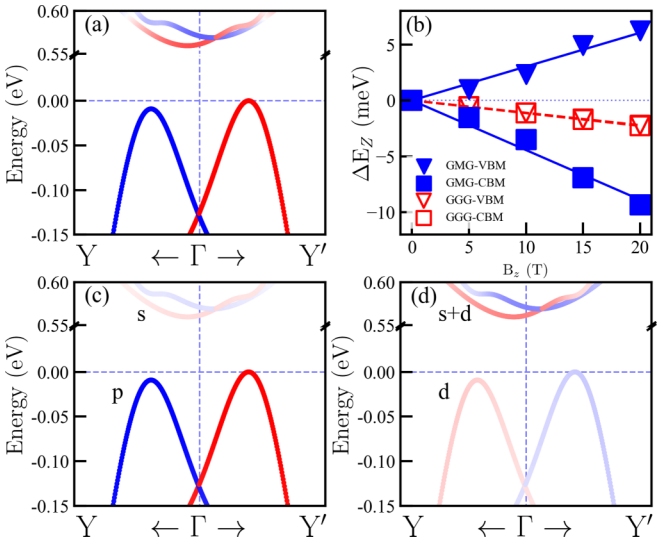

FIG. 4. (a) The band structure of GMG at Y-Γ-Y' under an out-of-plane magnetic field of 20 T, and (b) Zeeman-splitting energy as a function of out-of-plane magnetic field. (c) Te and (d) Mn projected band structure of panel (a). The color depth indicates the quantity of the projected contribution.

Finally, we construct a simplified band model including both Rashba-type and Zeeman effects based on a 2D free-electron approximation Hamiltonian:

$$H = H_0 + H_R + H_B = H_0 + \alpha_R k_y \sigma_z + \mu_B \boldsymbol{\sigma} \cdot \mathbf{B}, \tag{4a}$$

where

$$\mu_B \boldsymbol{\sigma} \cdot \mathbf{B} = \beta B_x \sigma_x + \gamma B_y \sigma_y + \eta B_z \sigma_z. \tag{4b}$$

Its eigenvalues are easily given as

$$E_\pm = E_0 \pm \sqrt{(\alpha_R k_y + \eta B_z)^2 + (\beta B_x)^2 + (\gamma B_y)^2}, \tag{4c}$$

where μ_B, σ, and B are the Bohr magneton, the Pauli matrix, and the magnetic flux density, respectively, while β, γ, and η are different parameters. When the external magnetic field is zero, i.e.,$\mathbf{B} = \mathbf{0}$, Eq. (4c) evolves into Eq. (2), which is the "normal" Rashba equation. When there is a magnetic field, both Rashba-type and Zeeman effects are included in Eq. (4c). Therefore, Eq. (4c) describes very well the novel effects in band structure involving both Rashba-type and Zeeman effects, and that we reveal here in GMG, SMS, GGG, and SSS.

In summary, we designed a specific 2D multiferroic material, namely, XMX, and conducted first-principles calculations on it. It is found that XMX possesses largely improved Rashba-type but also Zeeman effects, as compared to XXX fully made from XTe layers, which is particularly striking when realizing that large Rashba-type and Zeeman effects rarely coexist within the same system. The enhancement of the Rashba-type effect originates from the reduction of

thickness of XMX, which increases the interaction between surface states of the lowest conduction bands and neighboring states. The Zeeman effect is improved because of the *s-d* and *p-d* exchange interaction between Te and Mn ions. Our results therefore provide opportunities to realize a Majorana qubit in quantum information processing, topological superconductivity, and other promising phenomena requiring both relatively large Rashba-type and Zeeman effects.

The authors thank the National Key R&D Program of China (Grants No. 2022YFB3807601 and No. 2020YFA0711504), the National Science Foundation of China (Grants No. 11874207, No. 51725203, No. 51721001, No. 52003117, No. U1932115, and No. 12104416), the Program for Innovative Talents and Entrepreneur in Jiangsu (JSSCTD202101), and the Natural Science Foundation of Jiangsu Province (Grant No. BK20200262). C.X. and L.B. acknowledge the Vannevar Bush Faculty Fellowship (VBFF) Grant No. N00014-20-1-2834 from the Department of Defense and are thankful for support from the MonArk Quantum Foundry supported by the National Science Foundation Q-AMASE-i program under NSF Award No. DMR-1906383. We are grateful to the the HPCC resources of Nanjing University for the calculations.

[1] R. M. Lutchyn, J. D. Sau, and S. Das Sarma, Phys. Rev. Lett. **105**, 077001 (2010).
[2] V. Mourik, K. Zuo, S. M. Frolov, S. R. Plissard, E. P. A. M. Bakkers, and L. P. Kouwenhoven, Science **336**, 1003 (2012).
[3] S. M. Albrecht, A. P. Higginbotham, M. Madsen, F. Kuemmeth, T. S. Jespersen, J. Nygård, P. Krogstrup, and C. M. Marcus, Nature (London) **531**, 206 (2016).
[4] M. M. Desjardins, L. C. Contamin, M. R. Delbecq, M. C. Dartiailh, L. E. Bruhat, T. Cubaynes, J. J. Viennot, F. Mallet, S. Rohart, A. Thiaville, A. Cottet, and T. Kontos, Nat. Mater. **18**, 1060 (2019).
[5] R. Aguado and L. P. Kouwenhoven, Phys. Today **73**(6), 44 (2020).
[6] E. Prada, P. San-Jose, M. W. A. de Moor, A. Geresdi, E. J. H. Lee, J. Klinovaja, D. Loss, J. Nygård, R. Aguado, and L. P. Kouwenhoven, Nat. Rev. Phys. **2**, 575 (2020).
[7] Y.-J. Wu, J. Hou, Y.-M. Li, X.-W. Luo, X. Shi, and C. Zhang, Phys. Rev. Lett. **124**, 227001 (2020).
[8] N. P. de Leon, K. M. Itoh, D. Kim, K. K. Mehta, T. E. Northup, H. Paik, B. S. Palmer, N. Samarth, S. Sangtawesin, and D. W. Steuerman, Science **372**, eabb2823 (2021).
[9] A. Fornieri, A. M. Whiticar, F. Setiawan, E. Portolés, A. C. C. Drachmann, A. Keselman, S. Gronin, C. Thomas, T. Wang, R. Kallaher, G. C. Gardner, E. Berg, M. J. Manfra, A. Stern, C. M. Marcus, and F. Nichele, Nature (London) **569**, 89 (2019).
[10] A. Assouline, C. Feuillet-Palma, N. Bergeal, T. Zhang, A. Mottaghizadeh, A. Zimmers, E. Lhuillier, M. Eddrie, P. Atkinson, M. Aprili, and H. Aubin, Nat. Commun. **10**, 126 (2019).
[11] S. Vaitiekėnas, G. W. Winkler, B. van Heck, T. Karzig, M.-T. Deng, K. Flensberg, L. I. Glazman, C. Nayak, P. Krogstrup, R. M. Lutchyn, and C. M. Marcus, Science **367**, eaav3392 (2020).
[12] K. Rechcińska, M. Król, R. Mazur, P. Morawiak, R. Mirek, K. Łempicka, W. Bardyszewski, M. Matuszewski, P. Kula, W. Piecek, P. G. Lagoudakis, B. Piętka, and J. Szczytko, Science **366**, 727 (2019).
[13] C. Betthausen, T. Dollinger, H. Saarikoski, V. Kolkovsky, G. Karczewski, T. Wojtowicz, K. Richter, and D. Weiss, Science **337**, 324 (2012).
[14] J. M. Lu, O. Zheliuk, I. Leermakers, N. F. Q. Yuan, U. Zeitler, K. T. Law, and J. T. Ye, Science **350**, 1353 (2015).
[15] J. Krempaský, S. Muff, F. Bisti, M. Fanciulli, H. Volfová, A. P. Weber, N. Pilet, P. Warnicke, H. Ebert, J. Braun, F. Bertran, V. V. Volobuev, J. Minár, G. Springholz, J. H. Dil, and V. N. Strocov, Nat. Commun. **7**, 13071 (2016).
[16] F. E. Meijer, A. F. Morpurgo, T. M. Klapwijk, T. Koga, and J. Nitta, Phys. Rev. B **70**, 201307(R) (2004).
[17] D. Shcherbakov, P. Stepanov, S. Memaran, Y. Wang, Y. Xin, J. Yang, K. Wei, R. Baumbach, W. Zheng, K. Watanabe, T. Taniguchi, M. Bockrath, D. Smirnov, T. Siegrist, W. Windl, L. Balicas, and C. N. Lau, Sci. Adv. **7**, eabe2892 (2021).
[18] P. E. Blöchl, Phys. Rev. B **50**, 17953 (1994).
[19] G. Kresse and J. Furthmüller, Phys. Rev. B **54**, 11169 (1996).
[20] G. Kresse and J. Hafner, Phys. Rev. B **47**, 558 (1993).
[21] G. Kresse and J. Furthmüller, Comput. Mater. Sci. **6**, 15 (1996).
[22] J. P. Perdew, K. Burke, and M. Ernzerhof, Phys. Rev. Lett. **77**, 3865 (1996).
[23] S. L. Dudarev, G. A. Botton, S. Y. Savrasov, C. J. Humphreys, and A. P. Sutton, Phys. Rev. B **57**, 1505 (1998).
[24] V. I. Anisimov, F. Aryasetiawan, and A. I. Lichtenstein, J. Phys.: Condens. Matter **9**, 767 (1997).
[25] See Supplemental Material at http://link.aps.org/supplemental/10.1103/PhysRevB.106.L201105 for details about the stability, the methods, the band structure, and the competition versus collaboration between Rashba and Zeeman effects, and the magnetoelectric coupling of GMG and SMS can be found in the Supplemental Material.
[26] J. Heyd, G. E. Scuseria, and M. Ernzerhof, J. Chem. Phys. **118**, 8207 (2003).
[27] H. J. Monkhorst and J. D. Pack, Phys. Rev. B **13**, 5188 (1976).
[28] R. D. King-Smith and D. Vanderbilt, Phys. Rev. B **47**, 1651 (1993).
[29] J. Neugebauer and M. Scheffler, Phys. Rev. B **46**, 16067 (1992).
[30] E. Bousquet, N. A. Spaldin, and K. T. Delaney, Phys. Rev. Lett. **106**, 107202 (2011).
[31] M. Ye and D. Vanderbilt, Phys. Rev. B **89**, 064301 (2014).
[32] M. Ye and D. Vanderbilt, Phys. Rev. B **92**, 035107 (2015).
[33] H. Tian, L. Bellaiche, and Y. Yang, Phys. Rev. B **100**, 220103(R) (2019).
[34] T. Bayaraa, Y. Yang, M. Ye, and L. Bellaiche, Phys. Rev. B **103**, L060103 (2021).
[35] L. Chen, C. Xu, H. Tian, H. Xiang, J. Íñiguez, Y. Yang, and L. Bellaiche, Phys. Rev. Lett. **122**, 247701 (2019).
[36] C. Xu, P. Chen, H. Tan, Y. Yang, H. Xiang, and L. Bellaiche, Phys. Rev. Lett. **125**, 037203 (2020).

[37] K. Chang, J. Liu, H. Lin, N. Wang, K. Zhao, A. Zhang, F. Jin, Y. Zhong, X. Hu, W. Duan, Q. Zhang, L. Fu, Q.-K. Xue, X. Chen, and S.-H. Ji, Science **353**, 274 (2016).
[38] D. Kriegner, K. Výborný, K. Olejník, H. Reichlová, V. Novák, X. Marti, J. Gazquez, V. Saidl, P. Němec, V. V. Volobuev, G. Springholz, V. Holý, and T. Jungwirth, Nat. Commun. **7**, 11623 (2016).
[39] D. J. O'Hara, T. Zhu, A. H. Trout, A. S. Ahmed, Y. K. Luo, C. H. Lee, M. R. Brenner, S. Rajan, J. A. Gupta, D. W. McComb *et al.*, Nano Lett. **18**, 3125 (2018).
[40] S. Pal, R. Arora, S. Roychowdhury, L. Harnagea, K. Saurabh, S. Shenoy, D. V. S. Muthu, K. Biswas, U. V. Waghmare, and A. K. Sood, Phys. Rev. B **101**, 155202 (2020).
[41] N. V. Morozova, I. V. Korobeynikov, and S. V. Ovsyannikov, Appl. Phys. Lett. **118**, 103903 (2021).
[42] H. Yu and Y. Chen, J. Phys. Chem. C **122**, 15673 (2018).
[43] M. Liebmann, C. Rinaldi, D. Di Sante, J. Kellner, C. Pauly, R. N. Wang, J. E. Boschker, A. Giussani, S. Bertoli, M. Cantoni *et al.*, Adv. Mater. **28**, 560 (2016).
[44] C. Rinaldi, S. Varotto, M. Asa, J. Sławińska, J. Fujii, G. Vinai, S. Cecchi, D. Di Sante, R. Calarco, I. Vobornik *et al.*, Nano Lett. **18**, 2751 (2018).
[45] D. Di Sante, P. Barone, R. Bertacco, and S. Picozzi, Adv. Mater. **25**, 509 (2013).
[46] J. Krempaský, H. Volfová, S. Muff, N. Pilet, G. Landolt, M. Radović, M. Shi, D. Kriegner, V. Holý, J. Braun *et al.*, Phys. Rev. B **94**, 205111 (2016).
[47] Here we use the effective thickness $3d/2$ to compute the polarization, because the distribution of electron clouds is considered.
[48] Y. Zhang, J. Sun, J. P. Perdew, and X. Wu, Phys. Rev. B **96**, 035143 (2017).
[49] J. Schliemann, Rev. Mod. Phys. **89**, 011001 (2017).
[50] H. Djani, A. C. Garcia-Castro, W.-Y. Tong, P. Barone, E. Bousquet, S. Picozzi, and P. Ghosez, npj Quantum Mater. **4**, 51 (2019).
[51] K. Yamauchi, P. Barone, and S. Picozzi, Phys. Rev. B **100**, 245115 (2019).
[52] S. Singh and A. H. Romero, Phys. Rev. B **95**, 165444 (2017).
[53] K. Ishizaka, M. S. Bahramy, H. Murakawa, M. Sakano, T. Shimojima, T. Sonobe, K. Koizumi, S. Shin, H. Miyahara, A. Kimura *et al.*, Nat. Mater. **10**, 521 (2011).
[54] Y. Ma, Y. Dai, W. Wei, X. Li, and B. Huang, Phys. Chem. Chem. Phys. **16**, 17603 (2014).
[55] I. P. Rusinov, I. A. Nechaev, S. V. Eremeev, C. Friedrich, S. Blügel, and E. V. Chulkov, Phys. Rev. B **87**, 205103 (2013).
[56] M. S. Bahramy, R. Arita, and N. Nagaosa, Phys. Rev. B **84**, 041202(R) (2011).
[57] M. Kim, J. Ihm, and S. B. Chung, Phys. Rev. B **94**, 115431 (2016).
[58] P. B. Luiz Gustavo Davanse da Silveira and S. Picozzi, Phys. Rev. B **93**, 245159 (2016).
[59] L. L. Tao and E. Y. Tsymbal, Nat. Commun. **9**, 2763 (2018).
[60] M. I. Dyakonov and V. I. Perel, Sov. Phys. Solid State **13**, 3023 (1972).
[61] Z. Liao, P. Jiang, Z. Zhong, and R.-W. Li, npj Quantum Mater. **5**, 30 (2020).
[62] C. Hermann and C. Weisbuch, Phys. Rev. B **15**, 823 (1977).
[63] D. A. Bussian, S. A. Crooker, M. Yin, M. Brynda, A. L. Efros, and V. I. Klimov, Nat. Mater. **8**, 35 (2009).
[64] J. H. Yu, X. Liu, K. E. Kweon, J. Joo, J. Park, K.-T. Ko, D. W. Lee, S. Shen, K. Tivakornsasithorn, J. S. Son *et al.*, Nat. Mater. **9**, 47 (2010).
[65] J. K. Furdyna, J. Appl. Phys. **64**, R29 (1988).
[66] J. Gaj, in *Semiconductors and Semimetals* (Elsevier, New York, 1988), Vol. 25, pp. 275–309.